Associated conference: 5th International Small Sample Test Techniques Conference

Conference location: Swansea University, Bay Campus

Conference date: 10th - 12 July 2018

FE modelling of small punch creep test using Kocks-Mecking-Estrin model

H.K. Al-Abedy*, I.A. Jones and W. Sun

Faculty of Engineering, University of Nottingham, Nottingham NG7 2RD, UK
* Corresponding Author: E-mail address: Hiydar.Al-Abedy@nottingham.ac.uk

Abstract: Small punch creep testing (SPCT) of thin disc specimens can be considered as a useful technique for determination of creep properties of exposed components of power generation. In this work, the Kocks-Mecking-Estrin (KME) constitutive model is used to simulate the small punch creep behaviour of the P91 steel at 600℃ based on a full set of experimental results. An implicit computational algorithm is developed based on the radial return mapping approach. Finite element analyses of a small punch creep test is carried out using ABAQUS software coupled with a UMAT material subroutine which has been developed by the authors. The small punch creep test results are compared with the corresponding results from modelling using the UMAT code. In addition, a comparison of results of the uniaxial tensile test for the P91 steel at 600℃ with the corresponding modelling results is also presented. The numerical results obtained have shown the model's versatility and good predictive capability for the P91 steel at 600℃.

Keywords: Small Punch Creep Test; Visco-Plasticity; Kocks-Mecking-Estrin Model; Finite Element Method

Nomenclature

b	The magnitude of dislocation Burgers vector	t	Time
C_{ijkl}	Stiffness matrix tensor	t_s	The thickness of small punch specimen
d	Punch diameter	T	Temperature
D	Receiving hole diameter	α	Constant
G	Shear modulus	μ	Friction coefficient
k	Boltzmann constant	ε^p, $\dot{\varepsilon}^p$, $\dot{\varepsilon}^c$	Plastic strain, plastic and creep strain rates
k_1	Dislocation storage constant	$\dot{\bar{\varepsilon}}^p$	Effective plastic strain rate
k_2	Recovery coefficient	$\dot{\varepsilon}_o$	Reference strain rate
k_{20}	Constant	$\dot{\varepsilon}_{ij}, \dot{\varepsilon}_{ij}^e, \dot{\varepsilon}_{ij}^c$	Total, elastic and creep strain rate tensors
m	The exponent of stress sensitivity	$\dot{\bar{\varepsilon}}^c$	Effective creep strain rate
M	Taylor factor	ρ	Dislocation density
n	Dynamic recovery exponent	σ_s	Saturation stress
$\mathbb{N}_{ij}$	Flow direction tensor	$\hat{\sigma}$	Flow stress
p	Creep exponent	$\tilde{\sigma}$	Effective stress
$P1$	Punch load magnitude	σ_{ij}	Stress Tensor
$P2$	Punch clamp magnitude	$\hat{\sigma}_{so}$	The saturation stress value properties
r	Corner radius of holder and support	θ_o	The initial strain hardening at the second stage.
S	The diameter of small punch specimen	ω	Time interpolation parameter
S_{ij}	Deviatoric stress tensor	Λ	Strain hardening constant

1. Introduction

In the last ten years, testing techniques using miniature samples have received increasing attention from the electricity generation industry companies for situations where the amount of material used in the test is limited. Published reviews for small specimen techniques have focused on their applications to conventional and nuclear plants [1, 2]. The removal of small amounts of material that are required for miniature specimen testing may not affect the structural integrity of in-service components. FE analysis of small specimen tests has the potential to make them more acceptable as a means of in-service testing of power plant materials [3, 4]. The ease of manufacture and testing of SPCT samples is one of the most important characteristics that distinguish it from other miniature testing

techniques. SPCT has one more advantage over other miniature testing techniques, namely that the SPCT can evaluate creep rupture [5].

Historically, more viscoplasticity models have been obtained and used to model the creep of materials. One of the most popular and well-received models is the Kocks–Mecking–Estrin (KME) model for secondary creep which has been developed for a wide range of materials [6]. The constitutive equation describes the viscoplasticity law relating to von Mises equivalent stress and plastic strain rate quantities for a given microstructure [7, 8].

Many numerical types of research have used constitutive models such as that proposed by Kachanov [9], which take account of the typical creep curve. Abendroth [10] used an FE approach but focused on the modelling guidelines: the geometry of the SPT, the convergence of the chosen mesh and the influence of friction coefficient on a load-deflection curve. Manahan et al. [11] developed a modified plasticity approach to simulate creep curves and compare them with the corresponding experimental data by minimising the sum of the squares to determine the parameters of the model. FE modelling of small punch specimens was also proposed by Shibli et al. to justify the conception of the creep behaviour [12]. Evans and Evans have made use of an extended visco-plasticity model of SPCT to take into account the effect of surface morphology [13].

In the present work, in an attempt to overcome some of the repeatability issues, the KME viscoplastic model is implemented without the need to carry out a uniaxial creep test. The results of the FE analysis for uniaxial tensile, small punch creep tests using the KME model are compared with experimental results to investigate the capability of the numerical model to provide creep behaviour for the small punch creep test.

This paper is structured as follows: the second section presents a brief reminder of the constitutive equations of the Kocks-Mecking-Estrin (KME) model which are based on macrostructure properties. The development of the user material subroutine (UMAT) is widely detailed in this section. The implementation of the constitutive model, in the implicit finite element code ABAQUS/Standard, is also presented. The third section details the material and microstructure of the P91 steel. The uniaxial tensile and small punch creep tests for the P91 steel at 600⁰C for several loads are presented as well. The fourth section of this paper is devoted to the application of the model by characterising the material using uniaxial tensile and small punch creep cases. These simulations are used to validate the accuracy of the UMAT by comparing numerical modelling and corresponding experimental tests. Finally, conclusions are discussed in the last section.

2. The Kocks-Mecking-Estrin Model and UMAT Development

2.1 The Kocks-Mecking-Estrin Model

The Kocks-Mecking-Estrin form is a unified elasto-viscoplastic constitutive model which is highly nonlinear and referred to as the kinetic equation by Kocks [6] and Mecking [14]. An appropriate mathematical formulation has been suggested by Kocks [6]:

$$\dot{\bar{\varepsilon}}^p = \dot{\varepsilon}_o \left(\frac{\widetilde{\sigma}}{\widehat{\sigma}}\right)^m \tag{1}$$

where $\dot{\bar{\varepsilon}}^p$ is effective plastic strain rate, $\dot{\varepsilon}_o$ is a reference strain rate which is proportional to the mobile dislocation density, $\widetilde{\sigma}$ is effective stress, and m is an exponent of stress sensitivity. The quantity of flow stress, an internal state variable, $\widehat{\sigma}$, represents the microstructural state of a material which is related to the total dislocation density ρ [15]:

$$\widehat{\sigma} = \alpha bGM\sqrt{\rho} \tag{2}$$

Here α is a constant, b is the magnitude of dislocation Burgers vector, G is the shear modulus, and M is the Taylor factor. The model assumes that the micromechanical strength of the material is due to piling up of dislocation-dislocation interactions.

The evolution of the dislocation density takes into account the athermal process as well as the dynamic recovery process of dislocations in the uniaxial loading [16].

$$d\rho = M[k_1\rho^{1/2} - k_2\rho]d\varepsilon^p \tag{3}$$

Here k_1 is a constant accounting for the dislocation storage and k_2 is the recovery coefficient which represents the thermal process for the low temperature or high-temperature case. In both cases, it can be written as [16]:

$$k_2 = k_{20}\left(\frac{\dot{\varepsilon}^p}{\dot{\varepsilon}_o}\right)^{-1/n} \tag{4}$$

where k_{20} is a constant. In the above formulation, the dynamic recovery exponent n can be written as

$$n = \frac{\Lambda}{kT} \tag{5}$$

Equation (5) shows that n is inversely proportional to absolute temperature T, where k is the Boltzmann constant and Λ is the work hardening parameter [6].

The constitutive equations of this model can be integrated with the case of constant plastic strain rate [14] and with constant stress creep [15].

$$\frac{d\sigma}{d\varepsilon} = (\sigma/m)\frac{d\ln\dot\varepsilon}{d\varepsilon} + \left(\sigma/\hat\sigma\right)\frac{d\hat\sigma}{d\varepsilon} \tag{6}$$

At the steady state, the evolution of $\hat\sigma$ does not change with the strain $\left(\frac{d\hat\sigma}{d\varepsilon} = 0\right)$, the Equation (6) may provide a simple discerption of deformation in a creep. Substituting Equation (1) into Equation (6) gives

$$\frac{d\ln\left(\frac{\dot\varepsilon}{\dot\varepsilon_s}\right)}{d\varepsilon} = \left(\frac{\theta_o m}{\hat\sigma}\right)\left[\left(\frac{\dot\varepsilon}{\dot\varepsilon_s}\right)^{-1/n-1/m} - 1\right] \tag{7}$$

where θ_o is the initial strain hardening within the second stage and $\dot\varepsilon_s$ is steady state strain rate.

One of the essential goals of this work is to utilise the strain rate as a function of strain in creep tests at constant stress. The steady state strain rate $\dot\varepsilon_s$ corresponding to $\frac{d\dot\varepsilon}{d\varepsilon} = 0$ is given

$$\dot\varepsilon_s = \dot\varepsilon_o^{m/(m+n)}\dot\varepsilon_o^{n/(m+n)}\left(\frac{\sigma}{\alpha bGM\left(\frac{k_1}{k_{20}}\right)}\right)^{mn/(m+n)} \tag{8}$$

One can simplify Equation (8) to give

$$\dot\varepsilon_s = \dot\varepsilon_o\left(\frac{\sigma}{\hat\sigma_{so}}\right)^p \tag{9}$$

where $\frac{m}{(m+n)} + \frac{n}{(m+n)} = 1$ and $\frac{1}{p} = \frac{1}{m} + \frac{1}{n}$

2.2   The Multi-Axial Formulation

The one-dimensional constitutive equations for the Kocks-Mecking model have been derived by Estrin [17]. In this section, the significant aspects of the 3-dimensional version are discussed.

Since in most cases of experimental tests, the materials have shown nonlinear behaviour, the stress state, σ_{ij}, is assumed to be a nonlinear function of the strain state, ε_{ij}. Thus, using Hooke's law in chain rule form, these can be re-expressed as a direct notation to gives

$$\dot\sigma_{ij} = C_{ijkl}\dot\varepsilon_{kl}^e \tag{10}$$

where $\dot\sigma_{ij}$, $\dot\varepsilon_{kl}^e$ are the Cauchy stress rate and elastic strain rate tensor respectively (a superposed dot refers to the time derivative) while C_{ijkl} is the fourth order elastic stiffness matrix tensor which depends on the strain, but not on the strain rate.

$$C_{ijkl} \equiv \frac{\partial\sigma_{ij}}{\partial\varepsilon_{kl}} \tag{11}$$

In elasto-viscoplasticity, it is usual to split the total strain rate tensor, $\dot\varepsilon_{ij}$, into two parts, namely an elastic strain rate, $\dot\varepsilon_{ij}^e$ and a creep strain rate tensor, $\dot\varepsilon_{ij}^c$, i.e.

$$\dot\varepsilon_{ij} = \dot\varepsilon_{ij}^e + \dot\varepsilon_{ij}^c \tag{12}$$

The update of $\dot\varepsilon_{ij}^e$ is given by

$$\dot\varepsilon_{ij}^e\big|_{n+1} = \dot\varepsilon_{ij}^e\big|_n + \left(\Delta\varepsilon_{ij} - \Delta\varepsilon_{ij}^c\right) \tag{13}$$

The elastic strain rate tensor can be connected with the rate form of Hooke's law, Equation (12), to give:

$$\dot{\sigma}_{ij}\big|_{n+1} = C_{ijkl} : \left(\dot{\varepsilon}_{ij}^e\big|_n + \Delta\varepsilon_{ij} - \Delta\varepsilon_{ij}^c\right) \tag{14}$$

To derive the incremental constitutive relationship, let us consider an integration over one step, Δt, from $t|_n$ to $t|_{n+1}$.

$$\sigma_{ij}\big|_{n+1} = \sigma_{ij}\big|_n + C_{ijkl}:\Delta\varepsilon_{ij} - C_{ijkl}:\Delta\varepsilon_{ij}^c\big|_{n+1} \tag{15}$$

$$\sigma_{ij}\big|_{n+1} = \sigma_{ij}^{tr} - C_{ijkl}:\Delta\varepsilon_{ij}^c\big|_{n+1} \tag{16}$$

where σ_{ij}^{tr} is an elastic predictor which is known and obtained by assuming the increment is entirely elastic, while $\Delta\varepsilon_{ij}^c$ are the creep strain increments [18].

In the following, we assume that the creep strain rate $\dot{\varepsilon}_{ij}^c$ is expressed using the Levy-von Mises equation as [19]:

$$\dot{\varepsilon}_{ij}^c = \dot{\tilde{\varepsilon}}^c \, \mathbb{N}_{ij} \ , \ \mathbb{N}_{ij} = \frac{3}{2}\frac{S_{ij}}{\tilde{\sigma}} \tag{17}$$

where $\dot{\tilde{\varepsilon}}^c$ is the effective creep strain rate, $\mathbb{N}_{ij}$ is the flow direction tensor, and S_{ij} denotes the deviatoric stress tensor, while the quantities in Equation (18) indicate the equivalent stress and equivalent creep strain rate respectively.

$$\tilde{\sigma} = \sqrt{\frac{3}{2}S_{ij}:S_{ij}} \ , \text{ and } \dot{\tilde{\varepsilon}}^c = \sqrt{\frac{2}{3}\dot{\varepsilon}_{ij}^c:\dot{\varepsilon}_{ij}^c} \ , \tag{18}$$

2.3   The UMAT Coding and Implementation

The FE software ABAQUS permits the addition and implementation of various constitutive models into the ABAQUS library by using user material subroutines (UMATs) [20]. In the present study, the Kocks-Mecking-Estrin constitutive model described above for constant stress creep is implemented into ABAQUS by UMAT for the P91 steel at 600°C.

We here presented the implicit backward Euler integration for the multiaxial case of equations in the previous section. According to Equation (9), the rate form of the constitutive equation may be written in an incremental form as

$$\Delta\tilde{\varepsilon}^c = \Delta t \, \phi(\mathcal{F})^p \tag{19}$$

and thus may be expressed in a form suitable for Newton-Raphson iterative solution as [21]

$$\mathcal{R}(\Delta\tilde{\varepsilon}^c) = \Delta t \, \phi(\mathcal{F})^p - \Delta\tilde{\varepsilon}^c = 0 \tag{20}$$

Using Newton's method, one has

$$\mathcal{R} + \frac{\partial\mathcal{R}}{\partial\tilde{\varepsilon}^c}\,\delta\varepsilon^c = 0 \tag{21}$$

In this method, an additional iteration step i is introduced to calculate the increment in accumulated creep strain that gives $\mathcal{R}(\Delta\tilde{\varepsilon}^c) = 0$
The first step, $i = 0$ (initial) $\Delta\tilde{\varepsilon}_0^c = 0$

$$\mathcal{R}_0 = \mathcal{R}(\Delta\tilde{\varepsilon}_0^c) \tag{22}$$

at the next step, (i) is replaced with $(i+1)$, so Equation (21) becomes [21]:

$$\delta\tilde{\varepsilon}^c\big|_{i+1} = -\frac{\mathcal{R}\big|_i}{\frac{\partial\mathcal{R}}{\partial\tilde{\varepsilon}^c}\big|_{\Delta\tilde{\varepsilon}_i^c}} \tag{23}$$
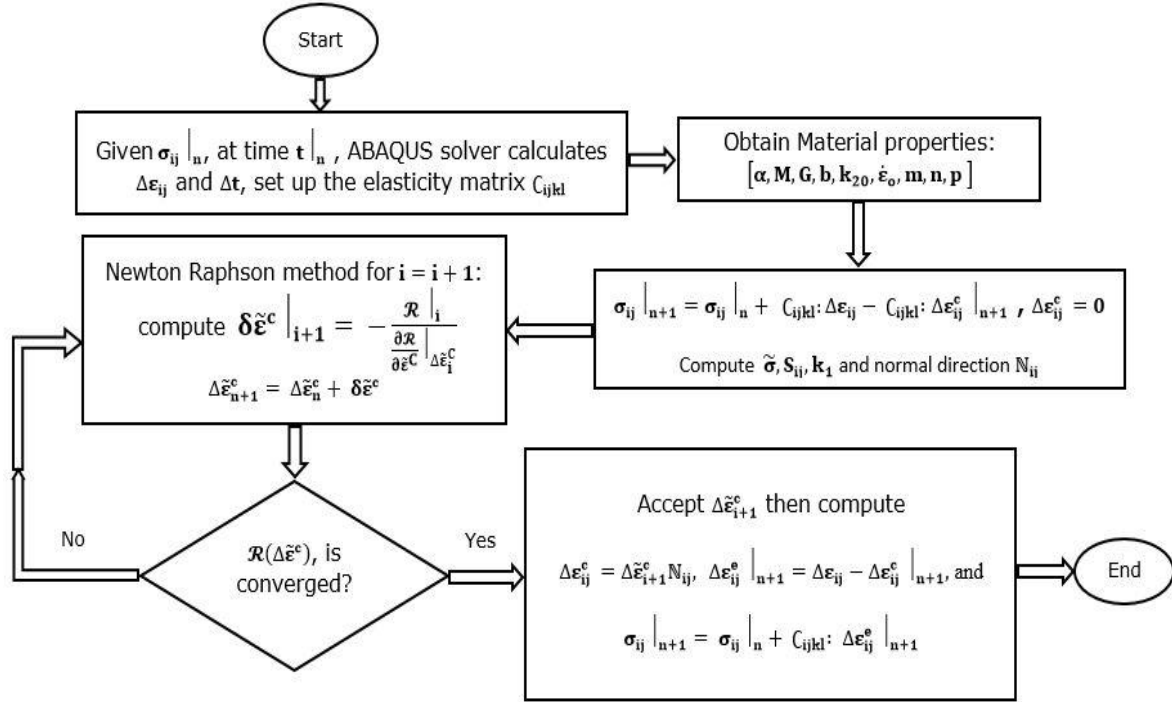
Now, the effective creep strain increment is updated by

$$\Delta\tilde{\varepsilon}_{n+1}^c = \Delta\tilde{\varepsilon}_n^c + \delta\tilde{\varepsilon}^c \tag{24}$$

The final step is to update the stress by

$$\sigma_{ij} \big|_{n+1} = \sigma_{ij} \big|_{n} + C_{ijkl} : \Delta\varepsilon_{ij}^{e} \big|_{n+1} \tag{25}$$

The flow chart of the implementation of the UMAT for the Kocks-Mecking-Estrin (KME) model is shown in Figure 1.

Figure 1. Flowchart of the implementation of the UMAT for KME model.

2.4   Material Jacobian Matrix

The material Jacobian can be described as a partial derivative

$$C_{ijkl} \equiv \frac{\partial\sigma_{ij}}{\partial\varepsilon_{kl}} = C_{ijkl}^{e} + C_{ijkl}^{cr} \tag{26}$$

A closed-form solution to C_{ijkl}^{e} the elastic stiffness matrix always knows. A closed-form solution to C_{ijkl}^{cr} the creep stiffness matrix may or may not know. Reversing the creep stiffness matrix, C_{ijkl}^{cr}, will furnish the creep compliance matrix, S_{ijkl}^{cr}, as given

$$S_{ijkl}^{cr} = \left(C_{ijkl}^{cr}\right)^{-1} = \frac{\partial\Delta\varepsilon_{ij}^{cr}}{\partial\Delta\sigma_{kl}} \tag{27}$$

The matrix was simplified to the following

$$S_{ijkl}^{cr} = \frac{\partial\Delta\varepsilon_{ij}^{cr}}{\partial\Delta\sigma_{kl}} = \frac{3}{2}\dot{\varepsilon}_{o}\,\hat{\sigma}_{so}^{-p}\Delta t\left[(p-1)\tilde{\sigma}^{p-2}\frac{\partial\tilde{\sigma}}{\partial S_{pq}}S_{ij} + \tilde{\sigma}^{p-1}\delta_{ip}\delta_{jq}\right]\frac{\partial S_{pq}}{\partial\Delta\sigma_{kl}}. \tag{28}$$

To obtain the stiffness matrix the compliance tensor must be inverted

$$C_{ijkl}^{cr} = \left(S_{ijkl}^{cr}\right)^{-1} \tag{29}$$

3. Experimental Work on P91 Steel at 600ºC

3.1   The P91 Material and Microstructure

Experimental tensile and small punch creep tests were presented for the P91 steel at 600ºC. The material chemical composition of the P91 steel used in the current work exhibits in Table 1. Figure 2a shows EBSD image of the virgin material microstructure.

Table 1. The chemical composition of the P91 steel [3].

Cr	Mo	C	Si	S	P	Al	V	Nb	N	W	Fe
8.60	1.02	0.12	0.34	0.002	0.017	0.007	0.24	0.070	0.060	0.030	Bal

3.2   Uniaxial Tensile Test

The conventional uniaxial tensile specimen is manufactured from a P91 pipe. The gauge length of the sample is 50mm, and the diameter of the gauge length is 10mm. The dimensions of the tensile specimen are shown in Figure 2b. The complete stress-strain curve obtained from the uniaxial tensile test at 600ºC. The Young's modulus of P91 steel is determined to be 145GPa at 600ºC, while the elongation of the specimen is 18% at the fracture.
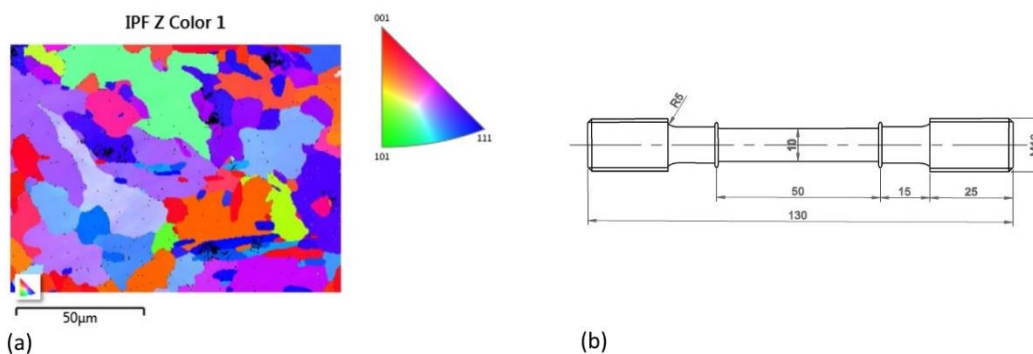

Figure 2. (**a**) EBSD texture of the virgin P91 steel used for the tests. (**b**) A uniaxial tensile test specimen, all dimensions in mm.

4. Modelling the Uniaxial Tensile and SPC Tests Using the Kocks-Mecking-Estrin Equations.

4.1   Modelling of Uniaxial Tensile Test

FE modelling of the uniaxial tensile test of the P91 steel at 600ºC was carried out using the UMAT coding via ABAQUS standard. The mesh of specimen consists of 673 axisymmetric quadrilateral elements. Only a quarter section was modelled due to symmetry. By including the geometrically non-linear effect, the uniaxial tensile specimen can induce significant deformation and neck with large localised strains. Figure 3 is a contour plot of the von-Mises stress at failure for a strain rate of $0.0005s^{-1}$, while Figure 4 shows the stress/strain curves obtained using the UMAT with the KME model and the corresponding tensile test carried out for the P91 steel at 600ºC. The material constant α, the magnitude of dislocation Burgers vector b, and Taylor factor M were taken from [22], these and other previous material constants used in calculations for the P91 steel are listed in Table 2.
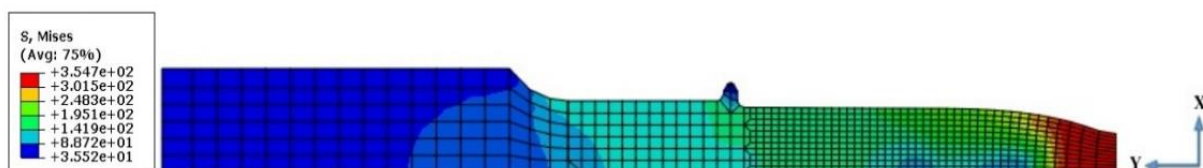
Figure 3. Contour plot of the von-Mises stress at failure for the P91 steel at 600ºC.
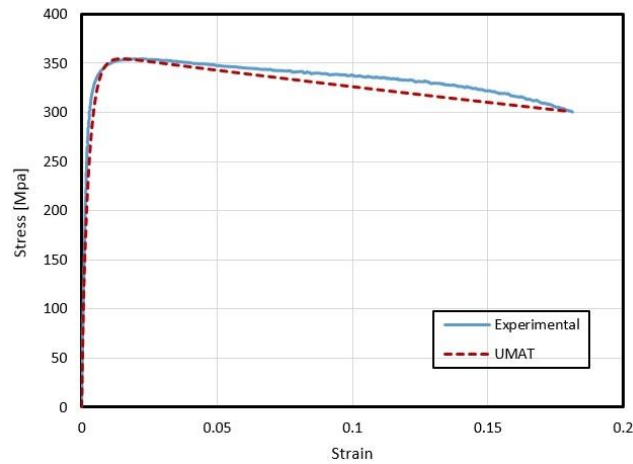
Figure 4. Experimental and numerical FE stress-strain curves for the P91 steel at 600ºC.

**Table 2.** Notation and material constants used in numerical FE for the P91 steel at 600ºC [22].

| Parameter	Name	Value
ρ_i	Initial Dislocation Density	1×10^{14} m^{-2}
v	Poisson's ratio	0.3
b	The magnitude of Burgers vector	2.5×10^{-10} m
m	The exponent of stress sensitivity	55.89
$\dot{\varepsilon}_o$	Reference strain rate	1 s^{-1}
k_{20}	Dynamic recovery	55
α	Constant	0.8
M	Taylor factor	3.06

4.2 Modelling of Small Punch Creep Tests

i. FE Model

Finite element modelling of small punch creep for P91 steel at 600℃ was carried for five levels of punch loads P1= 25, 28, 30, 34 and 40 kg using the UMAT code and the material properties given in Table 2. Figure 5 shows the geometry of the FE model where the punch radius (d/2) is 1.04mm, the holder and the support radius (r) is 0.25mm, the thickness (t_s), and radius of the specimen (S/2) are 0.5 and 4mm, respectively, the receiving hole radius (D/2) is 2mm. The punch, the holder, and the support were modelled as rigid bodies. Approximately half of the surface of the bottom of the specimen is constrained by a support to simulate being clamped between surfaces. The friction coefficient between these surfaces is assumed to be 0.8 [23]. The sample was implemented as a deformable body modelled using two different type of elements: the majority of the elements (1480) are 4-noded bilinear axisymmetric quadrilaterals with reduced integration (CAX4R), with transitions to zones of refined mesh involving ten 3-noded axisymmetric triangle elements (CAX3). The specimen was refined along the contact region between the punch and the sample. Figure 6 shows the mesh used for the SPCT analysis and the minimum element size, in the refined zone, is 0.025mm. The contacting interfaces between the top surface of the sample with rigid punch were assigned as a surface to surface contacts with a coefficient of friction assumed to have a value of 0.2 thus value being chosen from a parametric study described later in this section. The simulation was carried out with three types of boundary conditions. Firstly, the axial movement and rotation around the axis of symmetry of the support were constrained entirely. Secondly, the horizontal movement and rotation of punch and holder were also restricted to zero. The complete displacement and rotation constraints were applied on the left side of the specimen in the X-direction for all nodes located on the Y-axis. The loads are directed in the Y direction and are applied to the reference point of rigid punch that can represent the whole stiff punch, while a clamping load, 500N, is used on to the reference point of the holder die.
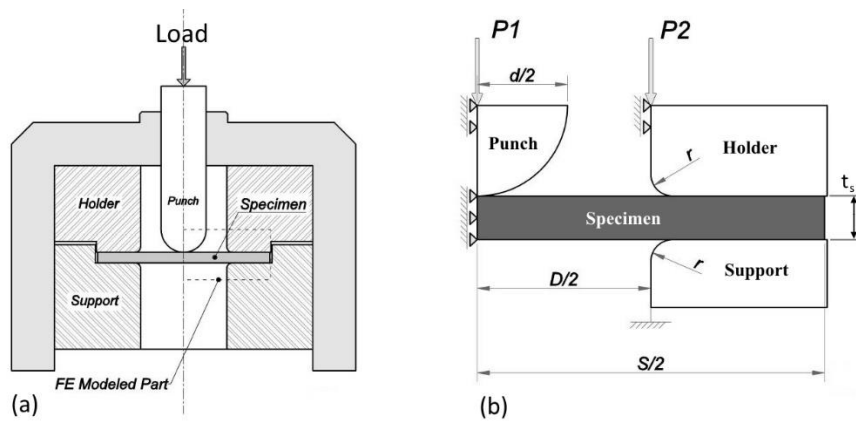
Figure 5. Schematic representation of a FE model for small punch creep testing analysis (D=4mm, S=8mm, d=2.08mm, r=0.25mm, t_s=0.5mm). (**a**) Schematic two-dimensional of rig for small punch creep testing. (**b**) Representation loads and boundary conditions of finite element modelled part.
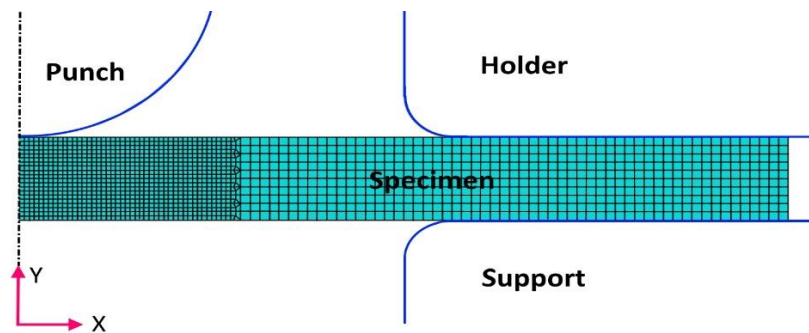

Figure 6. FE mesh used for SPCT specimen.

ii. Displacement-Time Curves

The parametric study of the different friction coefficients between the specimen and punch is carried out. The contact between the sample and punch was modelled using a surface to surface contact with various friction coefficients. Figure 7 shows the effect of friction coefficient for three values (μ = 0.2, 0.3 and, 0.4) with two cases of loads 34 and 40kg, respectively. It can be observed clearly that the effect of the coefficient of friction on the FE outputs is significant and the value of the friction coefficient of $μ = 0.2$ that gives the best approximation between modelling and practical data. The relationship between the coefficient of friction and the magnitude of the friction forces is directly proportional. For a given load levels, when the friction coefficient increases, the minimum deflection rate will drop and the failure time will increase.
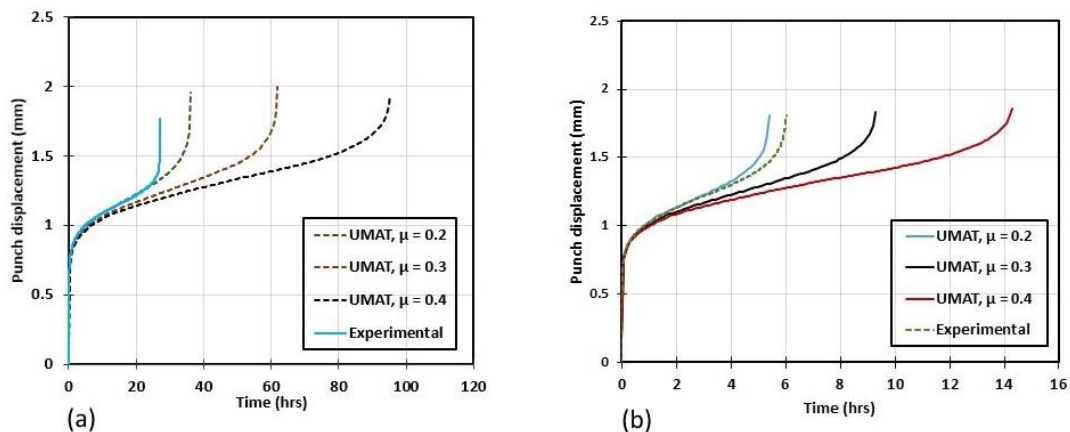
Figure 7. Calculated SPCT curve at the variation of the friction coefficient for punch load (**a**) 34Kg and, (**b**) 40Kg.

The experimental SPCT curves at five different load levels and the corresponding predicted curves are compared in Figure 8. The FE simulations using the proposed model show good agreement with the corresponding experimental results. The coefficient of friction between punch and specimen is assumed to be constant ($\mu = 0.2$) for all applied loads. During the first SPCT regime, the sample undergoes a severe change in shape. Change of the structure causes a decrease in the specimen's stiffness and a change in the deformation mechanism, from bending dominated to 'membrane stretching' dominated. In the second SPCT regime, the controlling mechanism is tensile stretching of the annular region around the contact edge between the punch and the specimen. Material creep damage is still acceptable to occur in the secondary SPCT region. The third SPCT region, symbolised by developing deformity rate, is governed by creep material degradation and specimen necking.
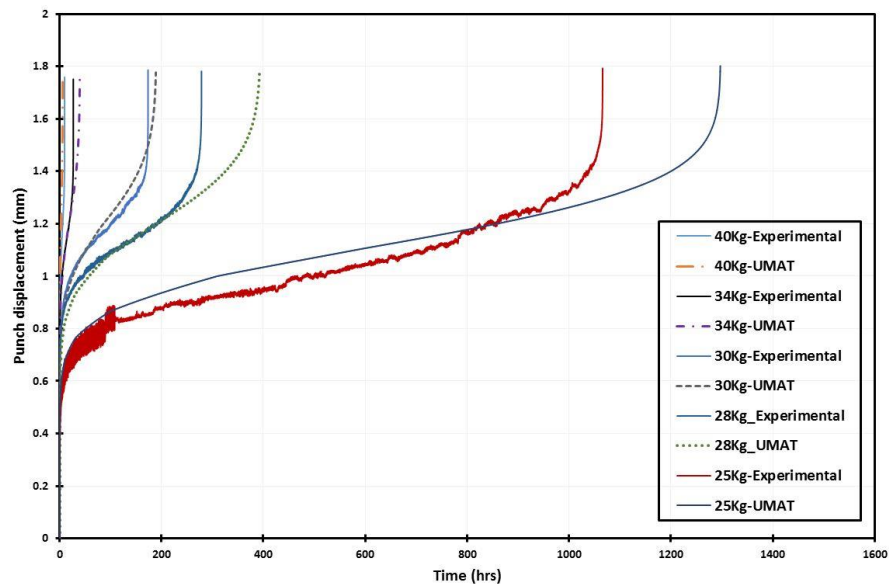
Figure 8. The experimental and calculated SPCT curves at punch load of 25, 28, 30, 34, and 40Kg [3].

iii. Contours of Displacement, von Mises Stress and Strain

The FE analysis of SPCTs was carried out using UMAT code through the ABAQUS package. Figure 9a shows the results of punch deformation at load 34Kg. The displacement of the punch is about 1.403mm after a time of 19 hours. Figure 9b shows the distribution of stress at the cross-section of the specimen after 19 hours under a constant punch load of 34Kg. The highest equivalent stress value is observed at the zone is located over a distance of 0.9mm, for the whole specimen thickness, from the centre of the initial specimen at the start of SPC test (see Figure 5b). Increasing stress is also observed at the top of sample surface located at distance of 2.0mm from the centre of the sample as a result of the tension in that region. Figure 9c shows the variations of equivalent strain under applied loads of 34Kg. Equivalent strains show a sharp rise in the area located on the bottom surface of the specimen at distance of 0.55mm from the centre of the sample. This deformation may be due to severe bending of the specimen from continuous of punch movement towards down which may ultimately lead to failure. Except for this region, the maximum equivalent strains occur identically to the rest of specimen.
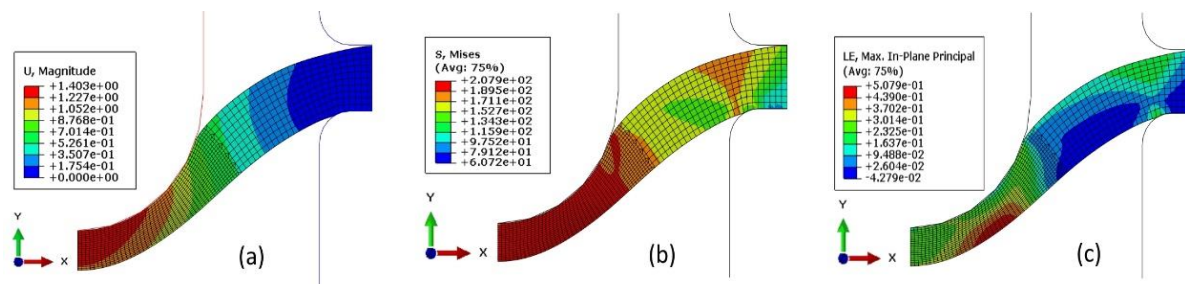
Figure 9. Contour plot of the SPCT at a punching load of 34Kg for (**a**) Punch direction deformation, (**b**) The equivalent stress and (**c**) The equivalent strains

Figure 10 shows SEM image of experimental SPC tests for punch load of P1= 25 kg which is postponed after 669 hours and the corresponding effective strain contour plots. The regions of local deformity were nearly identical to those of the experimental specimen tested. The directions and locations of the strain data are identified in Figures 9c and 10 where the effective strains at the weakest position do not change despite loading times increase.
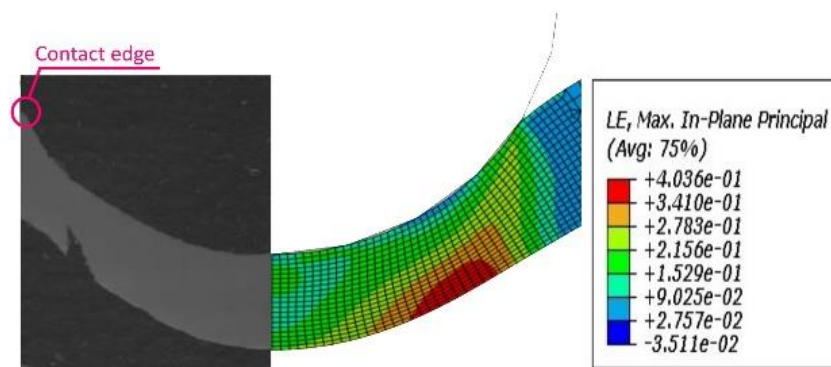
Figure 10. Contour plot of strain and SEM images of SPCT at punch load 25Kg for P91 steel at 600ºC.

5. Conclusions

The constitutive equations of KME model rely on the basic physical microstructure which was implemented by the finite element modelling through the user material subroutine (UMAT) and evaluated by the experimental results. The testing procedure involved SPCT, uniaxial tensile tests on the P91 steel at 600ºC.

For viscoplastic numerical simulations of SPC and uniaxial tensile tests under high forces, the KME modelling provides more accurate results with the experimental data at elevated temperatures.

The additional advantage of using the current model is the capability to determine the creep model parameters from utilizing microstructure information than uniaxial creep testing.

The influence of friction behaviour of the contact between punch and specimen was considered for SPCTs at different levels of load. The failure time gradually increases with an increase of the friction coefficient.

The maximum equivalent strain was observed within an annular zone on the underside of the specimen and this weakest location did not change even though loading time elapsed during SP creep testing analysis.

In the future work, the KME model will be extended to include material damage taking into account the effect of grain size. The determination of material parameters will be identified using a suitable optimisation strategy based on physical measurements.

References

1. Hyde, T.H.; Sun, W. and Williams, J.A. Requirements for and Use of Miniature Test Specimens to Provide Mechanical and Creep Properties of Materials: A Review. *Int Mater Rev.* **2007**, *52,* 213-255.
2. Morris, A.; Cacciapuoti, B. and Sun, W. The Role of Small Specimen Creep Testing within a Life Assessment Framework for High Temperature Power Plant. *Int Mater Rev.* **2018**, *63,* 102-137.

3. Cortellino, F.; Rouse, J.; Cacciapuoti, B.; Sun, W. and Hyde, T.H. Experimental and Numerical Analysis of Initial Plasticity in P91 Steel Small Punch Creep Samples. *Exp Mech.* **2017**, 1-20.
4. Rouse, J.; Cortellino, F.; Sun, W.; Hyde, T.H. and Shingledecker, J. Small Punch Creep Testing: Review on Modelling and Data Interpretation. *Mater Sci Tech.* **2013**, *29,* 1328-1345.
5. Dymáček, P. and Milička, K. Small Punch Testing and Its Numerical Simulations under Constant Deflection Force Conditions. *Strength Mater+* **2008**, *40,* 24-27.
6. Kocks, U. Laws for Work-Hardening and Low-Temperature Creep. *J Eng Mater Tech.* **1976**, *98,* 76-85.
7. Wu, Y.; Zhou, J.; Dong, S.; Hu, A.; Wang, L. and Pang, X. Constitutive Modeling for Strain Rate-Dependent Behaviors of Nanocrystalline Materials Based on Dislocation Density Evolution and Strain Gradient. *J Mater Res* **2014**, *29,* 2982-2993.
8. Barlat, F.; Glazov, M.; Brem, J. and Lege, D. A Simple Model for Dislocation Behavior, Strain and Strain Rate Hardening Evolution in Deforming Aluminum Alloys. *Int J Plasticity* **2002**, *18,* 919-939.
9. Kachanov, L. *Introduction to Continuum Damage Mechanics*; Springer Science & Business Media: USA, 2013.
10. Abendroth, M. FEM Analysis of Small Punch Tests. *Key Eng Mat.* **2017**, *734,* 23-36.
11. Manahan, M.; Browning, A.; Argon, A. and Harling, O. Miniaturized Disk Bend Test Technique Development and Application. In The Use of Small-Scale Specimens for Testing Irradiated Material, ASTM International, New Mexico, 1986.
12. Shibli, I.; Holdsworth, S. and Merckling, G. Creep and Fracture in High Temperature Components: Design and Life Assessment Issues. In ECCC Creep Conference, London, UK, 2005.
13. Evans, R. and Evans, M. Numerical Modelling of Small Disc Creep Test. *Mater Sci Tech.* **2006**, *22,* 1155-1162.
14. Mecking, H. and Kocks, U. Kinetics of Flow and Strain-Hardening. *Acta Metall Mater.* **1981**, *29,* 1865-1875.
15. Estrin, Y. and Mecking, H. A Unified Phenomenological Description of Work Hardening and Creep Based on One-Parameter Models. *Acta Metall Mater.* **1984**, *32,* 57-70.
16. Estrin, Y. Dislocation Theory Based Constitutive Modelling: Foundations and Applications. *J Mater Process Tech.* **1998**, *80,* 33-39.
17. Estrin, Y., Dislocation-Density-Related Constitutive Modelling, in *Unified Plastic Constitutive Laws of Deformation*, KRAUSZ, A.S. and KRAUSZ, K., Academic Press limited: London. 1996. 69-106, 0-12-425970.
18. Rezania, M.; Taiebat, M. and Poletti, E. A Viscoplastic Saniclay Model for Natural Soft Soils. *Comput Geotech* **2016**, *73,* 128-141.
19. Chaboche, J. A Review of Some Plasticity and Viscoplasticity Constitutive Theories. *Int J Plasticity* **2008**, *24,* 1642-1693.
20. ABAQUS, Analysis User's Manual Version 6.8. Hibbitt, Karlsson and Sorensen, Inc.: Pawtucket, USA, **2010**.
21. Dunne, F. and Petrinic, N. *Introduction to Computational Plasticity*, 2nd ed.; Oxford University Press: New York, USA, 2005.
22. Domkin, K. Constitutive Models Based on Dislocation Density: Formulation and Implementation into Finite Element Codes. PhD thesis, Luleå University of Technology, Sweden, 2005.
23. Cortellino, F.; Sun, W.; Hyde, T.H. and Shingledecker, J. The Effects of Geometrical Inaccuracies of the Experimental Set-up on Small Punch Creep Test Results. *J Strain Anal Eng.* **2014**, *49,* 571-582.